Arch. Metall. Mater. **63** (2018), 4, 1883-1888

DOI: 10.24425/amm.2018.125119

D. BOLIBRUCHOVÁ*#, R. PODPROCKÁ*, R. PASTIRČÁK*, K. MAJOR-GABRYŚ**

THE ROLE OF Mn IN ALUMINIUM ALLOYS WITH A HIGHER IRON CONTENT

The paper deals with the influence of manganese in AlSi7Mg0.3 alloy with higher iron content. Main aim is to eliminate harmful effect of intermetallic – iron based phases. Manganese in an alloy having an iron content of about 0.7 wt. % was graded at levels from 0.3 to 1.4 wt. %. In the paper, the effect of manganese is evaluated with respect to the resulting mechanical properties, also after the heat treatment (T6). Morphology of the excluded intermetallic phases and the character of the crystallisation of the alloy was also evaluated. From the obtained results it can be concluded that the increasing level of manganese in the alloy leads to an increase in the temperature of the β-Al_5FeSi phase formation and therefore its elimination. Reducing the amount of β-Al_5FeSi phase in the structure results in an improvement of the mechanical properties (observed at levels of 0.3 to 0.8 wt. % Mn). The highest addition of Mn (1.4 wt.%) leads to a decrease in the temperature corresponding to the formation of eutectic silicon, which has a positive influence on the structure, but at the same time the negative sludge particles were also present

Keywords: AlSi7Mg0.3, β-Al_5FeSi phase, manganese, thermal analysis

1. Introduction

Nowadays, the main requirements in the field of automotive castings is the cost reduction in order to achieve competitiveness while maintaining high quality. Al-Si secondary alloys are used for this purpose, which, in addition to cost and energy savings produce lower emissions compared to primary aluminium production (also more environmentally friendly). [1-4]. Iron is the most common impurity in Al-Si alloys, and with the presence of other elements in the alloy creates intermetallic compounds. Intermetallic iron-based phases that form during solidification can occur in various morphologies: such as β-Al_5FeSi-needle, α-Al_{15} (Fe, Mn) 3Si2 – Chinese script, polyhedral or skeleton formations. The amount, size and shape of these phases depends on the cooling rate, the chemical composition and the iron content in the melt. Phase Al_5FeSi (β-phase) is the most frequent observed compound that occurs in the form of thin plates or sticks and has a significant effect on final product properties. After exceeding the so-called the critical iron content, which is calculated from: $Fe_{crit} \approx 0{,}075 \times (\%Si) - 0{,}05$ [1] is even more significant. With higher iron contents as permitted by the material standard of the experimental alloy (0.5 to 1.2 wt. % Fe), the resulting phase can significantly reduce the tear strength due to higher brittleness and hardness compared to the aluminium matrix. At the same time, this phase is formed prior to the eutectic solidification and results in the occurrence of porosity in the castings. After increasing the iron level above the critical level, consideration should be given to the appropriate way to eliminate it. Manganese is an effective element to change needle-like intermetallic particles. After the addition of manganese, Al(FeMn)Si phases with a cubic crystallographic lattice are formed, which are predominantly present in the interdendritic regions and are excluded in the form of massive sharp skeleton formations, respectively so-called „Chinese scripts" that do not initiate cracks as the β-Al_5FeSi phase. According to previous research, the recommended ratio of the manganese addition to eliminate the negative effect of iron is unclear. Increasing the Mn / Fe ratio does not necessarily support β-phase precipitation on the α-phase ($Al_{15}(FeMn)_3Si_2$) [7]. There may be a risk of the nucleation of so-called sludge phases if a certain concentration of iron, manganese and chromium is present in the alloy, which is expressed by sludge factor – SF = 1x% Fe + 2x% Mn + 3x [1]. These phases do not arise during crystallization, but they are already present in the molten metal while maintaining the melt at low temperature or at rapid cooling of the melt [8,9].

2. Experimental procedure

As the experimental material AlSi7Mg0.3 alloy with higher iron content (marked as Ref.) was used. The main reason for the higher concentration of iron in the alloy as permitted by EN 1706 is the assumption of the formation of large iron-based intermetal-

* UNIVERSITY OF ŽILINA, FACULTY OF MECHANICAL ENGINEERING, DEPARTMENT OF TECHNOLOGICAL ENGINEERING, ŽILINA, SLOVAKIA
** AGH UNIVERSITY SCIENCE AND TECHNOLOGY, FACULTY OF FOUNDRY ENGINEERING, 23 REYMONTA STR., 30-059 KRAKOW, POLAND
# Corresponding author: danka.bolibruchova@fstroj.uniza.sk

lic phases in the microstructure and their better analysis after the addition of manganese. The aim was to analyse the real effect of Fe and Mn in secondary alloys (there are scientific disproportions and traditional approach is not sufficient). The alloy was properly contaminated with Fe. A higher iron content in the alloy (about 0.7 wt.% Fe) was achieved by adding AlFe10 master alloy. The traditionally recommended amount of manganese added to eliminate the harmful effect of iron is about Mn / Fe = 0.5. There are castings having a prescribed Mn / Fe ratio of greater than 0.7 [5]. From the above we can conclude that there are high-strength castings with higher Mn / Fe ratio than 0.7.

According to Table 1, the critical iron content Fe_{crit} (above 0.5) was exceeded in all alloys, therefore the occurrence of iron intermetallic phases in the microstructure and the decrease of mechanical properties due to the presence of these phases can be expected. At the same time, based on the calculation of the tendency of the alloy to form sludge phases according to SF, these formations may occur at higher manganese contents. Manganese was added in the form of AlMn20 master alloy in graduated levels of 0.3 wt. % Mn to 1.4 wt. % Mn. The chemical composition of the investigated alloys is shown in Table 1. Melting of each alloy was carried out by an electric resistance furnace in a graphite crucible. The samples were cast into a metallic mold heated to 200°C ±5°C at 760°C ±5°C. The alloys were not inoculated, modified or refined in any way before melts were carried out.

TABLE 1

Chemical composition of the secondary alloy AlSi7Mg0.3 after the addition of Mn

Alloy	Si	Fe	Mn	Mg	Cr	Ti	Sr	Fe_{crit}	Mn/Fe	SF
Ref.	7.093	0.099	0.072	0.38	0.002	0.18	0.015	0.48	0.73	0,25
AlSi7Mg0.3	7.310	0.778	0.071	0.299	0.001	0.135	0.011	0.50	0.09	0,92
AlSi7Mg0.3 + 0.3 wt. % Mn	7.046	0.743	0.474	0.381	0.002	0.139	0.0083	0.48	0.64	1,70
AlSi7Mg0.3 + 0.6wt. % Mn	6.916	0.753	0.699	0.36	0.0027	0.134	0.0043	0.47	0.93	2,16
AlSi7Mg0.3 + 0.8 wt. % Mn	7.083	0.684	0.704	0.35	0.0056	0.141	0.0077	0.48	1.03	2,11
AlSi7Mg0.3 + 1.0 wt. % Mn	6.670	0.585	0.874	0.347	0.0036	0.139	0.011	0.45	1.49	2,34
AlSi7Mg0.3 + 1.2 wt. % Mn	6.560	0.635	1.079	0.359	0.0047	0.139	0.0097	0.44	1.70	2,81
AlSi7Mg0.3 + 1.4 wt. % Mn	6.450	0.629	1.232	0.354	0.0057	0.135	0.0087	0.43	1.96	3,11

Samples for tensile testing and hardness testing were prepared from the castings. The tensile test was performed according to EN 42 0310 with a maximum load of 20 kN and a constant head speed of 2 mm / min with a test rod diameter 10 mm. Brinell's method was used to measure hardness. To evaluate the effect of graded Mn additions on the type and morphology of intermetallic compounds, samples were prepared by a standard metallographic procedure. Samples were etched with 20 ml of H_2SO_4 and 100 ml of water for light microscope, for SEM and EDX analysis solution with 0.5% HF. For deep etching was used 36 ml of HCl + 100 ml of H_20, the samples surface were etched for approximately 1.5 minutes. The process of crystallization of iron-based intermetallic phases in a secondary alloy with different manganese contents was evaluated by thermal analysis using a K-type (NiCr-Ni) thermocouple.

Subsequently, all samples were subjected to T6 heat treatment, which included annealing at 535°C ±5° for 6 hours, cooling in warm water at 50°C ±5° and artificial aging at 170°C ±5° for 4 hours.

3. Results and discussion

Fig. 1 shows the results of the tensile strength in the cast and after the heat treatment. The red and green lines on the graphs (Fig. 1 to 3) show the minimum required mechanical properties without and with T6 heat treatment for the AlSi7Mg0.3 alloy according to EN 1706. The higher iron content in the AlSi7Mg0.3

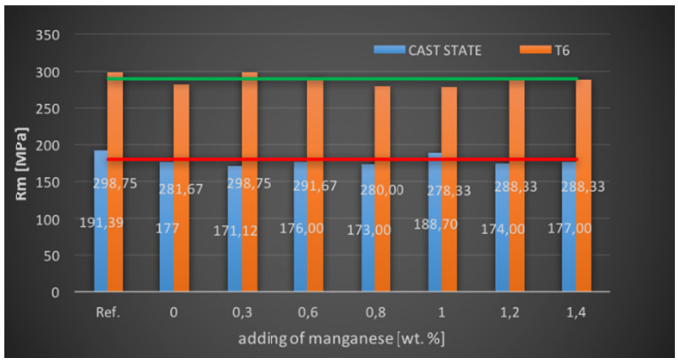

Fig. 1. Dependency of tensile strength of secondary alloy AlSi7Mg0.3 with graduated wt. % Mn without heat treatment and after heat treatment

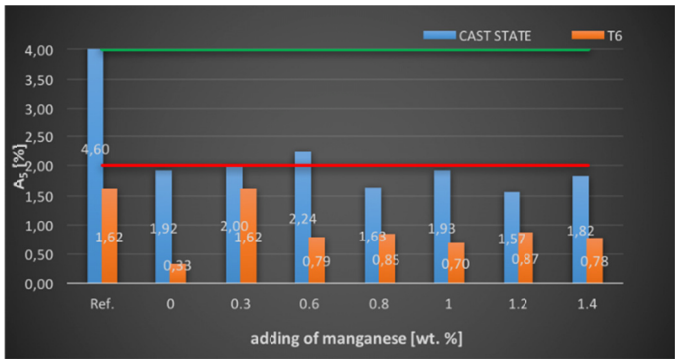

Fig. 2. Dependence of tensibility the secondary alloy AlSi7Mg0.3 with graded wt. % Mn without heat treatment and after heat treatment

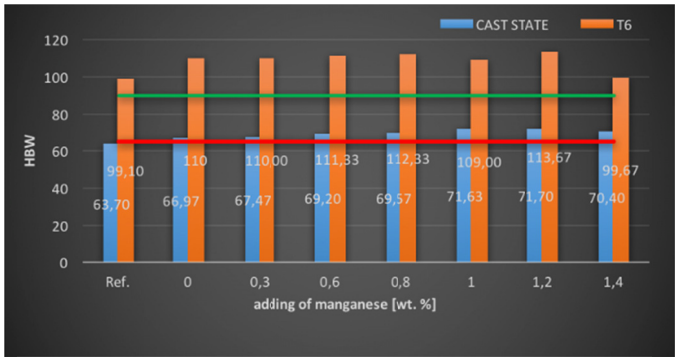

Fig. 3. Dependence of Brinell hardness the secondary alloy AlSi7Mg0.3 with graded wt. % Mn without heat treatment and after heat treatment

alloy caused a decrease in tensile strength and elongation compared to the reference (primary) alloy as prescribed by EN 1706. Up to 1.0 wt. % Mn tensile strength increases where it reaches the highest values and decreases after this addition. The average value of tensile strength without heat treatment after the addition of manganese is at 176 MPa at 0.3 and 0.6 wt. % Mn. The highest values of tensile strength after heat treatment were achieved with the addition of 0.3 wt. % Mn – 298.75 MPa and with 0.6 wt. % Mn reached value of 291.67 MPa. The highest improvement in ductility is observed with the addition of 0.3 wt. % Mn and 0.6 wt. % Mn in samples without heat treatment, the same applies to heat treated samples. From the hardness measurement results, it is clear that the higher iron content of the alloy and the increasing level of manganese, as predicted, resulted in an increase of alloy hardness.

Fig. 4a shows a typical microstructure of the secondary alloy AlSi7Mg0.3 in which the long intermetallic β-Al_5FeSi phase plate particles are evenly distributed in the interdendritic areas of the aluminium matrix and also along the eutectic silicon. Due to the very low level of Mn in the alloy, the skeletal particles are not present. In Fig. 4b it can be seen that after addition of 0.3 wt. % Mn is the excluded intermetallic β-Al_5FeSi phase present in smaller dimensions, with 0.6 wt. % also fragments of skeletal morphology are present (Fig. 4c).

After addition of 0.8 wt. % Mn phases in the form of smaller skeleton formations or "Chinese script" can be found in the structure. Individual elements in the alloy can be seen in the EDX image – Fig. 5. The intermetallic β-Al_5FeSi phase is

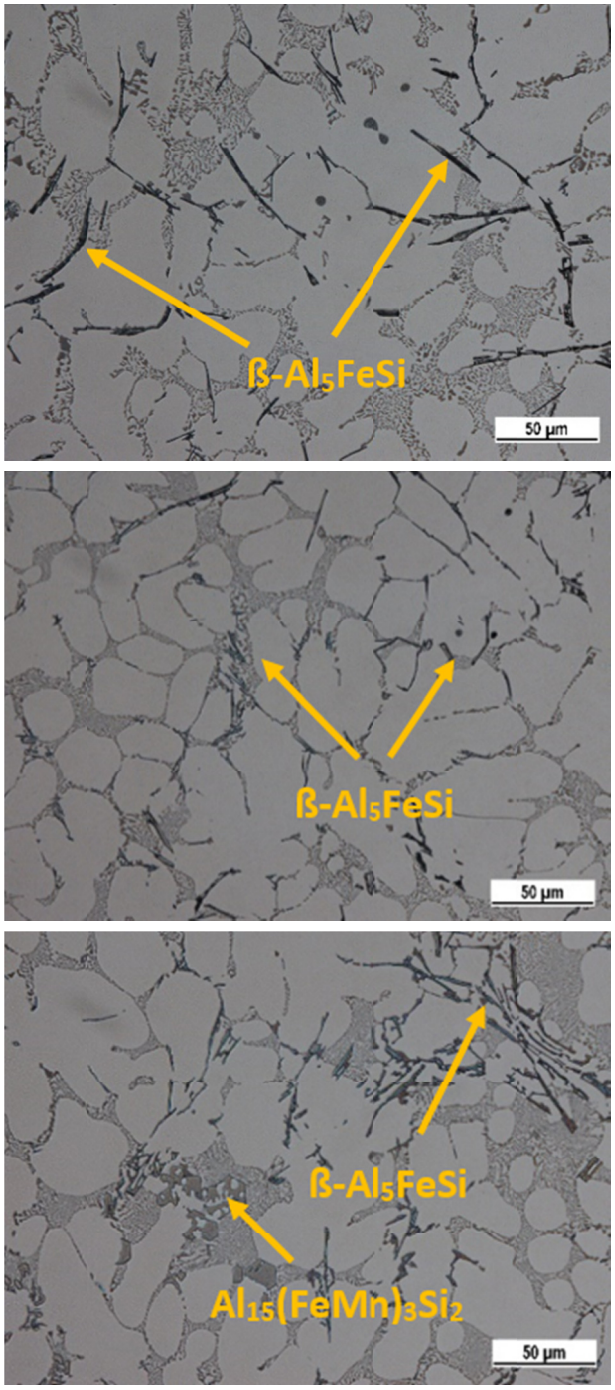

Fig. 4. Microstructure of secondary alloy AlSi7Mg0.3 (a) without addition of Mn (b) with the addition of 0.3 wt. % Mn (c) with the addition of 0.6 wt. % Mn

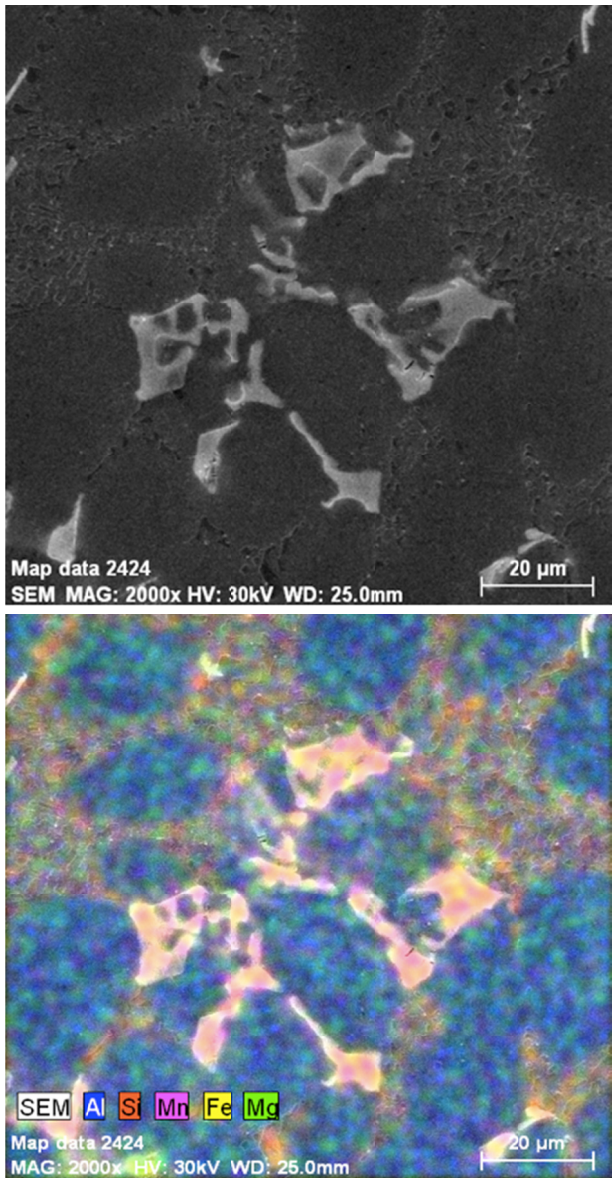

Fig. 5. Mapping of skeletal particle $Al_{15}(FeMn)_3Si_2$ phase of the secondary alloy AlSi7Mg0.3 after addition of 0.8 wt. % Mn (a) REM (b) mapping

present already with the very small amount of manganese, the higher content caused significant fragmentation of the β-Al_5FeSi phase plates (Fig. 6). After addition of 1.0 wt. % Mn the structure was the same as in the previous case (Fig. 7a). According to [3], the transformation effect of manganese is characterized by the reaction of $L + Al_5FeSi \rightarrow Al + Si + Al_{15}(FeMn)_3Si_2$ when the Al_5FeSi (β-phase) plates are transformed into $Al_{15}(FeMn)_3Si_2$ skeletal morphology or Chinese type eventually polyhedral crystals. For this reason, manganese content must be sufficient to prevent β-Al_5FeSi formation even in later stages of solidification. After increasing Mn to 1.2 wt. % Mn, long alumina structures of $Al_{15}(FeMn)_3Si_2$ are present in the alloy structure (Fig. 7b). At the highest level of Mn to 1.4 wt.%, Mn also sludge particles are present, mainly distributed in the aluminium matrix (Fig. 8).

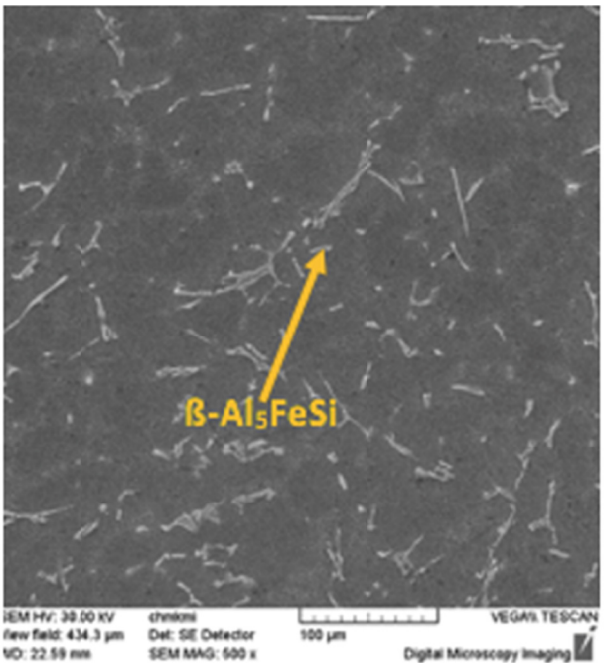

Fig. 6. Fragmentation of the plate particle β-Al_5FeSi in the secondary alloy AlSi7Mg0.3 after addition of 0.8 wt. % Mn

The thermal analysis was performed to evaluate the impact of wt. % Mn on the crystallization process of iron-based intermetallic phases and also on the excluded phases morphology. From the results of the thermal analysis (Fig. 9) it can be concluded that the combination of the higher iron content in the AlSi7Mg0.3 alloy with a graduated quantity of manganese resulted in an β-Al_5FeSi phase formation temperature increase. This increase is accompanied by the release of the heat. The critical iron value (see Table 1) was exceeded, which led to the formation of negative intermetallic compounds in the form of β-Al_5FeSi. With respect to the recommended Mn / Fe ratio (0.5), the β-Al_5FeSi phase was eliminated by shortening its length at value Mn / Fe = 0.64 (0.3% Mn – Fig. 4b). The most significant shortening of the length occurred at Mn / Fe > 0.93 (0.6 wt.% – Fig. 4c). Because of the ß-Al_5FeSi length shortening followed by the morphology changes to skeletal or Chinese script, 0.3 to

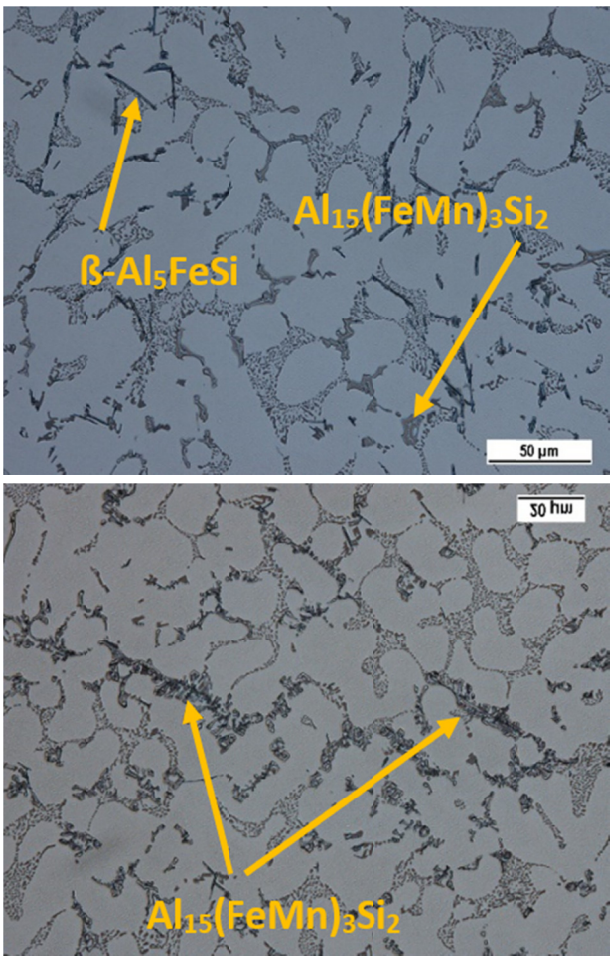

Fig. 7. Microstructure of secondary alloy AlSi7Mg0.3 (a) with 1.0 wt. % Mn (b) with 1.2 wt. % Mn

0.8 wt. % Mn achieved the best strength and elongation values. Structural changes were observed at Mn / Fe > 0.93 where the skeletal formations of the $Al_{15}(FeMn)_3Si_2$ phase (Fig. 4c) were already contained in the alloy structure. There was also a decrease in the temperature corresponding to the formation of eutectic silicon. At the highest level of manganese, the eutectic reaction time is prolonged and also eutectic silicon as well as the skeletal phases are influenced. The occurrence of sludge phases according to the SF calculations is expected with the addition of 0.6 wt. % Mn and SF of 2.16, but their presence is confirmed at SF > 2.81 (Fig. 7b). Increasing amounts of manganese led to a decrease of the solidification temperature, which could lead to formation of sludge phases observed at the highest level of manganese.

4. Conclusions

From the results of experimental measurements for AlSi7Mg0.3 alloy with a higher iron content than allowed by the material standard, it can be stated that the positive effect of manganese in the elimination of the negative intermetallic phase β-Al_5FeSi was confirmed. It was also confirmed that a higher Mn / Fe ratio than traditional recommendations is needed to

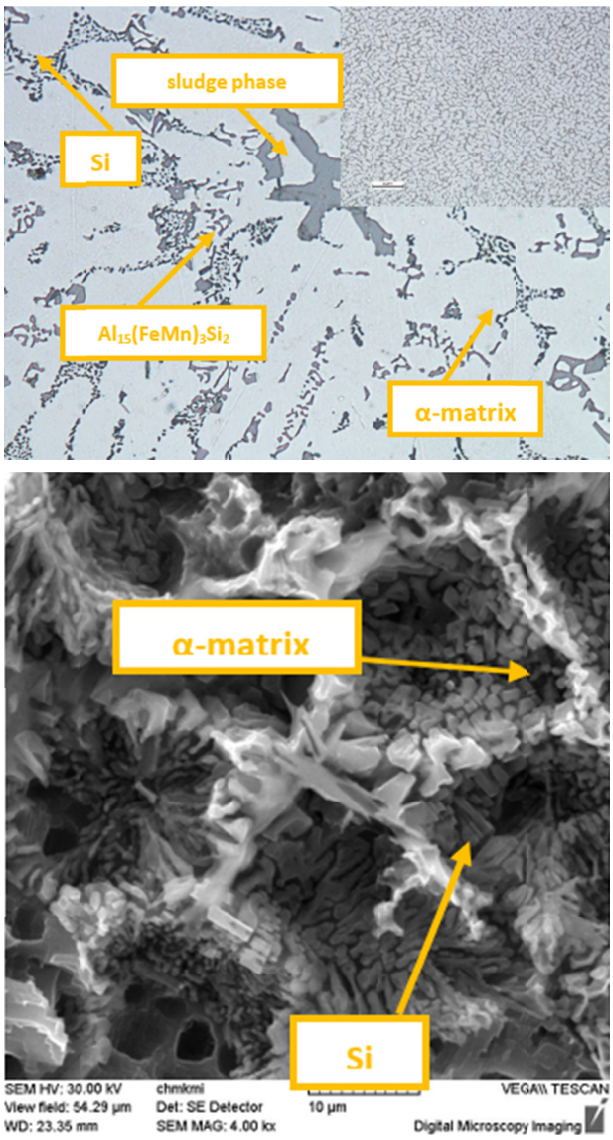

Fig. 8. Microstructure of secondary alloy AlSi7Mg0.3 with 1.4 wt. % Mn

obtain optimal mechanical characteristics. In our case, the best mechanical properties were achieved at a Mn / Fe ratio of >0.64, adding 0.3 to 0.8 wt. % Mn. The tensile strength and Brinell hardness reached the best values for samples without, but also with heat treatment (required by EN 1706 despite high iron concentrations in the batch). Required elongation values was not achieved after the heat treatment.

The paper points out the effect of the graduated amount of manganese on the AlSi7Mg0.3 secondary alloy crystallization process. Growing manganese content increased the β-Al_5FeSi phase formation temperature and with ratio Mn/Fe >0.64 shortening of the needle length and the morphology change was observed. By increasing the Mn amount in the alloy, the temperature of the eutectic silicon formation and the solidification temperature was reduced. At the highest Mn content, besides the influence on the iron intermetallic phases, influence on morphology of the eutectic silicon was also observed.

The results of the work also points out that even the high iron content in the alloy can be optimally corrected and applied for the castings that require high strength characteristics and hardness, but do not require high ductility values.

Acknowledgment

The authors thank VEGA SR for the financial support of this work, which is related to the solution of the grant assignment VEGA 1/0494/17.

REFERENCES

[1] J.A. Taylor, Proc. Mat. Sci. **1**, 19-33 (2012).

[2] D. Bolibruchová, J. Macko, M. Bruna, Arch. Metall. Mater. **59** (2), 717-721 (2014).

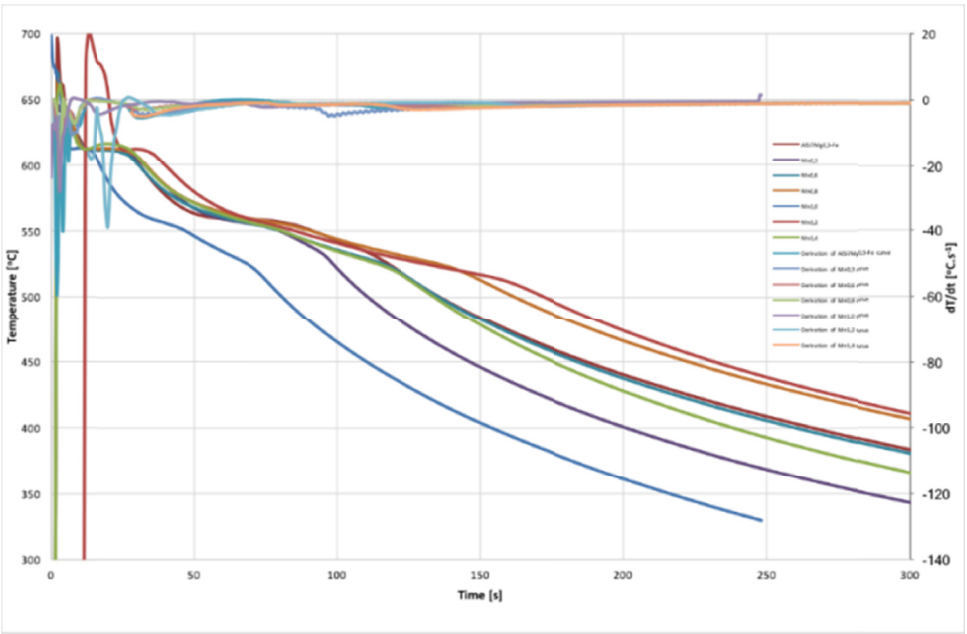

Fig. 9 Cooling curves and their first derivatives of the secondary alloy AlSi7Mg0.3 with graduated wt. % Mn

[3] S.G. Shabestari, Mater. Sci. Eng. A-Struct. **383** (2), 289-298 (2004)
[4] C. Dinnis, Scripta Mater. **53** (8), 955-958 (2005).
[5] R. Pastirčák, J. Ščury, American Institute of Physics Publising, **1745** (2016).
[6] M. Bruna, L. Richtarech, D. Bolibruchová, J. Caiss, Archives of Foundry Engineering **15** (2), 95-98 (2015).
[7] M. Mician, R. Konar. Archives of Foundry Engineering. **17** (3), 91-96, (2017).
[8] R. Konar, M. Mician, Archives of Foundry Engineering. **17** (2), 35-38, (2017).
[9] X. Cao, X, J. Campbell, Mater. Trans. **47** (5), 1303-1312 (2006).